Experimental and Theoretical Study of the Intrinsic Kinetics for Dimethyl Ether Synthesis from CO_2 over Cu–Fe–Zr/HZSM-5

Zu-zeng Qin, Tong-ming Su, and Hong-bing Ji
Guangxi Key Laboratory of Petrochemical Resource Processing and Process Intensification Technology, School of Chemistry and Chemical Engineering, Guangxi University, Nanning 530004, P.R. China

School of Chemistry and Chemical Engineering, Sun Yat-sen University, Guangzhou 510275, P.R. China

Yue-xiu Jiang and Rui-wen Liu
Guangxi Key Laboratory of Petrochemical Resource Processing and Process Intensification Technology, School of Chemistry and Chemical Engineering, Guangxi University, Nanning 530004, P.R. China

Jian-hua Chen
College of Resources and Metallurgy, Guangxi University, Nanning 530004, P.R. China

DOI 10.1002/aic.14743

An intrinsic kinetics model was established for CO_2 hydrogenation to dimethyl ether (DME) with a Cu–Fe–Zr/HZSM-5 catalyst based on H_2/CO_2 adsorption, simulation, and calculation of methanol synthesis from CO_2 intermediates and experimental data. H_2/CO_2-temperature programmed desorption results show a dissociative H_2 adsorption on Cu site; CO_2 was linearly adsorbed on Fe_3O_4 weak base sites of the catalyst; the adsorbing capacity of H_2 and CO_2 increased after Zr-doping. Density functional theory analysis of methanol synthesis from CO_2 and H_2 revealed a formate pathway. Methanol synthesis was the rate-limiting step (173.72 kJ·mol^{-1} activation energy) of the overall CO_2 hydrogenation reaction, and formation of H_2CO is the rate-determining step of methanol synthesis. Relative errors between calculated and experimental data of partial pressures of all components were less than 10%. Therefore, the kinetics model may be an accurate descriptor of intrinsic kinetics of CO_2 hydrogenation to DME. © 2015 American Institute of Chemical Engineers *AIChE J*, 61: 1613–1627, 2015

Keywords: carbon dioxide, dimethyl ether, catalytic hydrogenation, intrinsic kinetic

Introduction

With a high cetane number and a host of excellent chemical properties, dimethyl ether (DME) is not only a widely used chemical product but is also regarded as a potential clean energy fuel by virtue of its low NO_x content and the absence of SO_x components generated from it.[1,2] In recent years, the hydrogenation of CO_2 to form DME has been studied as an efficient method for converting CO_2 into a valuable chemical.[3–5] At present, there are two main processes for synthesizing DME from CO_2 and H_2, the first being a two-step process and the second a one-step process. Specifically, the two-step process consists of methanol synthesis followed by DME acquisition by way of methanol dehydration.

Three main reactions, show in Eqs. 1–3, describe the fundamental steps involved in these processes.

Methanol synthesis reaction:

$$CO_2+3H_2 \rightleftharpoons CH_3OH+H_2O \quad (\Delta H_{298}=-49.46\,\text{kJ}\cdot\text{mol}^{-1}) \tag{1}$$

Reverse water-gas shift reaction:

$$CO_2+H_2 \rightleftharpoons CO+H_2O \quad (\Delta H_{298}=41.17\,\text{kJ}\cdot\text{mol}^{-1}) \tag{2}$$

Methanol dehydration to DME:

$$2CH_3OH \rightleftharpoons CH_3OCH_3+H_2O \quad (\Delta H_{298}=-23.51\,\text{kJ}\cdot\text{mol}^{-1}) \tag{3}$$

In the one-step process, meanwhile, methanol synthesis and dehydration are completed in the same step. In this case, the thermodynamic equilibrium of the methanol synthesis process is broken,[6,7] allowing for a higher conversion rate per pass;[8] additionally, the combination of both steps into one improves the driving force of the reaction[7,9] and from an economic perspective, lowers the cost of equipment for large-scale synthesis.[10] For all of these reasons, the one-step process is the primary focus of developmental research into DME synthesis from CO_2.

At present, many studies regarding catalysts for and the underlying process of one-step synthesis of DME from CO_2 hydrogenation have been introduced in the literature and focus on Cu-based or Cu–ZnO-based catalysts for the hydrogenation step. Cu–Zn-based,[6,11–13] Cu–Mo,[14] Cu–Mn,[15] and

---

Correspondence concerning this article should be addressed to Z.-z. Qin at qinzuzeng@gmail.com, and H.-b. Ji at jihb@mail.sysu.edu.cn

$CuO–TiO_2–ZrO_2$[16] catalysts all exhibited good activity for CO_2 hydrogenation, with percent conversions of CO_2 and selectivity toward DME formation approximately 15–29 and 40–50%, respectively. However, DME synthesis generates more water than methanol synthesis alone, and as such, the activity and stability of catalysts could be adversely affected by the hydrophilicity of ZnO.[17,18] By considering recent research that used a CuO–ZnO-based catalyst in the catalysis of the one-step process[6,11] as well as reports of Cu–Fe-based catalysts that have been used to synthesize CO and CH_4,[19,20] and taking into account the fact that ZrO_2 is often used as a textural promoter,[11,21–23] a bifunctional catalyst was developed using $CuO–Fe_2O_3–ZrO_2$ as the methanol synthesis component and HZSM-5 as the methanol dehydration component.[24]

Up until this point, studies regarding the kinetic aspects of DME synthesis have focused on its generation from syngas: Iliuta et al.[25] have elucidated a model for DME synthesis in a fixed-bed membrane reactor, and Sierra et al.[26] investigated the deactivation kinetics for direct DME synthesis on a $CuO–ZnO–Al_2O_3/\gamma\text{-}Al_2O_3$ catalyst, among other works. Conversely, there have been very few reports on the kinetics governing the directed hydrogenation of CO_2 to DME. Through the study of kinetic models, McBride et al.[27] found that a layered catalyst arrangement significantly changes CO conversion as well as methanol and DME yield compared with a physical catalyst mixture, while Ereña et al.[6] considered deactivation of a $CuO–ZnO–Al_2O_3/\gamma\text{-}Al_2O_3$ catalyst during DME synthesis, and Zeng and coworkers[28,29] studied the intrinsic kinetics of DME synthesis directly from CO_2 hydrogenation over a $Cu–ZnO–SiO_2$/HZSM-5 and a $Cu–ZnO–Al_2O_3$/HZSM-5 catalyst. However, the reaction mechanism and the intrinsic kinetics model of CO_2 catalyzed hydrogenation to DME over Cu- or Cu–Zn-based catalysts are still uncertain, and the conversion of CO_2 and the selectivity of DME in general are still very low, and need to be improved. In this work, the adsorption of H_2 and CO_2 on the surface of the reported $CuO–Fe_2O_3–ZrO_2$ catalyst was studied by H_2-TPD, CO_2-TPD and was simulated using the DMol^3 module of Materials Studio. The process of catalyzed hydrogenation of CO_2 to synthesis methanol was also simulated and a kinetic model was established incorporating the elementary reactions above. The Langmuir–Hinshelwood (L-H) mechanism was used to investigate the pathway and intermediates of the reaction, and the restrictive effects of surface adsorption, chemical reaction, and desorption on the reaction rate. The rate-controlling step of methanol synthesis in the process of CO_2 hydrogenation was mainly discussed, and an intrinsic kinetics model, which was matched to the experimental data, was established, thereby yielding a mechanism for CO_2 hydrogenation to DME over a $CuO–Fe_2O_3–ZrO_2$/HZSM catalyst.

Experimental

Catalyst preparation

The $CuO–Fe_2O_3–ZrO_2$ mixed oxide catalyst was prepared by a coprecipitation method. $Cu(NO_3)_2·3H_2O$ and $Fe(NO_3)_3·9H_2O$ were weighed according to the Cu/Fe mole ratio of 3:2 and dissolved by deionized water followed by the addition of $Zr(NO_3)_4$ solution. The amount of the $Zr(NO_3)_4$ used depended on the desired ZrO_2 content of 1.0 wt % in $CuO–Fe_2O_3–ZrO_2$ (According to the literature,[24] the optimal doping amount of ZrO_2 found to be 1.0 wt %.). Under medium speed stirring, these nitrate solutions and a 1.0 mol·L^{-1} solution of Na_2CO_3 were added to a beaker using a parallel flow coprecipitating method while maintaining at pH of 10 and a reaction temperature of 70°C for 2 h. After being aged for 1 h, the mixture was filtered and dried at 110°C for 12 h, ground to 20–80 mesh and calcined at 400°C for 4 h, and the $CuO–Fe_2O_3–ZrO_2$ catalyst was obtained. HZSM-5 with a silica-alumina ratio of 300:1 (China Shanghai Novel Chemical Technology Co.) was mechanically mixed with the $CuO–Fe_2O_3–ZrO_2$ composite oxides at a 1:1 mass ratio. The preparation detail of Cu–Fe–Zr/HZSM-5 has been described previously in the literature.[24]

Catalyst characterization

H_2-TPD and CO_2-TPD experiments on the catalysts were performed using a PX200 multifunction catalyst analysis system (China Tianjin Golden Eagle Technology). For these analyses, 100 mg samples were reduced *in situ* at 300°C in a mixture of H_2 and Ar gases (8% H_2) at a flow rate of 30 mL·min^{-1} for 1 h, exposed to He (99.999%) flowing at 30 mL·min^{-1} for 1 h and then pumped to vacuum at 300°C for 1 h to remove any physically adsorbed species from the catalyst. After that, the sample was cooled to 50°C, and H_2 or CO_2 were introduced at 30 mL·min^{-1} for 0.5 h for dynamic absorption measurements of H_2 or CO_2. Subsequent static adsorption tests were performed at 0.2 MPa for 1.5 h to insure saturation adsorption of H_2 or CO_2. After that, gas desorption experiments were carried out in 30 mL·min^{-1} He (99.999%) in a range of 50–800°C with a ramp rate of 10°C·min^{-1}. The amount of gas desorbed was monitored by a thermal conductivity detector (TCD) held at 45°C.

Catalytic hydrogenation of CO_2 to DME

DME synthesis from CO_2 and H_2 was carried out in a fixed-bed reactor consisting of a stainless steel reaction tube with a 10 mm inner diameter and a 300 mm tube length. A total of 1.0 g $CuO–Fe_2O_3–ZrO_2$/HZSM-5 catalyst was loaded into the reactor and reduced at 300°C for 4 h in H_2 (99.999%) at a flow rate of 30 mL·min^{-1}. After the catalyst was reduced, the inflow of H_2 gas was replaced with a mixture of H_2 and CO_2 gases (5:1 mole ratio, respectively), and the catalytic hydrogenation of CO_2 to DME was performed within the ranges of 240–280°C and 2.0–4.0 MPa with a gaseous hourly space velocity within the range of 1,500–3,000 mL·g$_{cat}$$^{-1}$·h^{-1}. Under steady-state conditions, the products of DME synthesis were analyzed using an online Agilent 4890D gas chromatograph equipped with a TCD. The degree of CO_2 conversion and the selectivity to DME were calculated using a peak area normalization method.

Molecular simulation method

The adsorption state of CO_2 on a Cu(111) plane and the methanol synthesis process were studied using the DMol^3 module of Materials Studio (Accelrys Software), a modeling program that uses density functional theory (DFT).[30,31]

The unit cell of Cu is a face-centered cubic (FCC) lattice with a Fm3m space group. After structural optimization, obtained Cu lattice parameter (*a*) was 0.3685 nm, with a relative error of 1.94% when compared to the experimental values of 0.3615 nm,[32] indicating that the optimization method was rational. DFT and a generalized gradient slab model were used to simulate the adsorption configuration of CO_2

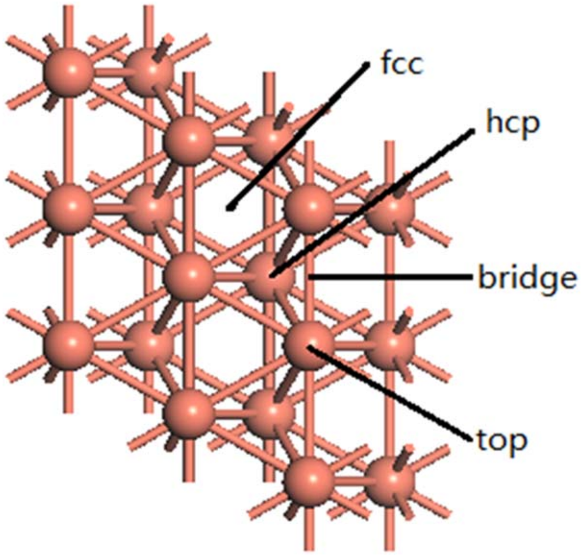

Figure 1. Schematic diagram of Cu(111) surface adsorption sites.

[Color figure can be viewed in the online issue, which is available at wileyonlinelibrary.com.]

molecules on the Cu(111) plane. Taking the accuracy and efficiency of the computation into account, it was established that the configuration of Cu(111) plane comprised two flat 3 × 3 supercells with an adsorbate coverage of 1/9 of a monolayer. The vacuum layer thickness was 1.5 nm, the bottom of the crystal was fixed, and the surface was relaxed and optimized. The CO_2 molecule was set to be linear, and the calculated value of the optimized C═O bond length was 0.1174 nm, which was consistent with the experimental value of 0.1162 nm.[33,34]

Eight possibilities for the adsorption of CO_2 onto the Cu(111) plane were built into the model as a combination of four adsorption positions on the Cu surface including atop, bridging, fcc (face-centered cubic site), and hcp (hexagonal-close-packed site)[35] sites (Figure 1) and either a vertical or horizontal CO_2 adsorption orientation. Optimized CO_2 molecules were moved to the top, bridge, fcc, and hcp position of the Cu(111) plane in one of the two configurations, and the adsorption configurations were then optimized. Energy, displacement, and force convergence were used as criteria for the structural optimization, and the threshold of convergence for each were 1×10^{-5} Ha (1 Ha = 627.51 kcal·mol^{-1}), 5×10^{-4} nm, and 2×10^{-2} Ha·nm^{-1}, respectively. The Monkhorst–Pack network parameter of the Brillouin-zone was set as 4 × 4 × 1, and the smearing factor found using the Methfessel–Paxton approximation was 0.005 Ha.

Adsorption energy E_{ads} is the change of the total energy of each substance before and after adsorption, calculated by Eq. 4.

$$E_{ads}=E_{(CO_2/surface)}-E_{(CO_2)}-E_{(surface)} \tag{4}$$

where, $E_{(CO_2/surface)}$ is the total energy of CO_2 adsorption on Cu(111) plane, $E_{(CO_2)}$ is the energy of a CO_2 molecule, and $E_{(surface)}$ is the energy of Cu(111) plane. E_{ads} can be thought to express the probability and the strength of adsorption: if E_{ads} is positive, the process is endothermic, in that the energy after adsorption is higher than the energy of the separate constituents, and the process is hard adsorption. Conversely, a negative E_{ads} indicates a process is exothermic, such that the adsorbate can be absorbed; the more negative the energy is, the more stable the adsorption system.

Results and Discussion

Temperature programmed desorption of H_2 and CO_2 from the Cu–Fe–Zr surface

H_2-TPD. After *in situ* reduction at 300°C, the CuO component of the Cu–Fe–Zr catalyst was converted to Cu, and Fe_2O_3 was converted to Fe_3O_4.[36] Subsequently, H_2-TPD was used to analyze the degree of H_2 adsorption on the Cu–Fe–Zr catalyst, and the results are shown in Figure 2.

Two hydrogen desorption regions are found in Figure 2: the high-temperature H_2 desorption peak (δ), which corresponds to hydrogen desorption from Fe adsorption sites, and the maximun temperature of the peaks were a little rasing from 334°C to approximately 340°C after ZrO_2 doping; and the lower temperature H_2 desorption peaks (α, β, and γ), which correspond to hydrogen desorption from Cu-based adsorption sites.[37,38]

To distinguish these kinds of hydrogen desorption in the H_2-TPD profiles of Cu–Fe and Cu–Fe–Zr catalysts, the H_2-TPD curves were fit into four bands with respect to desorption temperature. At least four stages of hydrogen desorption were observed, suggesting adsorption on sites with different degrees of interaction, which reflected in the temperatures required for desorption. The maximum temperature and peak area of each fitting peak are presented in Table 1. After doping with ZrO_2, the Zr-doping more than doubled the amount of hydrogen adsorbed, which suggests that ZrO_2 doping can increase the adsorption amount of H_2. The maximum temperatures of the desorption peaks α, β, and δ also increased from 150 to 163°C, 200 to 225°C, and 334 to 340°C, respectively. These results indicate that the adsorption of H_2 on the three types of sites was strengthened. Thus, a favorable environment for adsorption of higher concentrations of H_2 may be generated on the catalyst surface,[39] which would increase the reaction rate of CO_2 hydrogenation to DME.

As seen in Figure 2 and Table 1, the peak areas of type α adsorption on Cu (Cu–Fe catalyst at 150°C as well as Cu–Fe–Zr catalyst at 163°C) were minimal, and the amount of

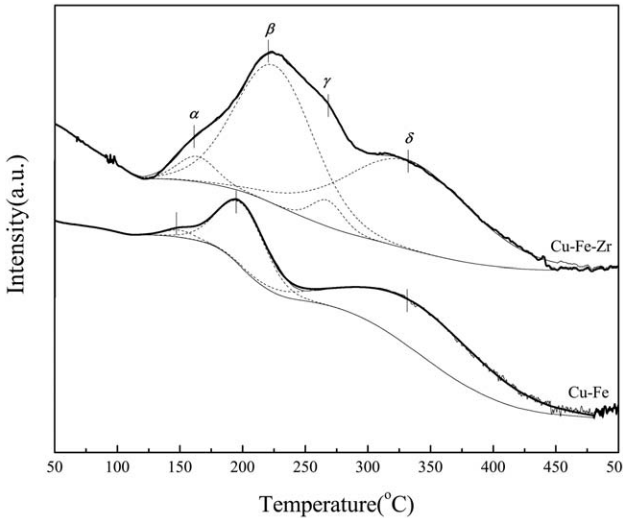

Figure 2. H_2-TPD profiles for Cu–Fe and Cu–Fe–Zr (ZrO_2 1.0 wt %).

Table 1. Maximum Temperatures and Area Distributions of the Four Gaussian Fitting Peaks (α, β, γ, and δ) of the H_2-TPD Profiles for Cu–Fe and Cu–Fe–Zr Catalysts

	α		β		γ		δ		
Catalysts	T (°C)	Area (unit)	T (°C)	Area (unit)	T (°C)	Area (unit)	T (°C)	Area (unit)	Total Area (unit)
Cu–Fe	150	8.8	200	126.4	–	–	334	263.1	398.3
Cu–Fe–Zr (1.0 wt %)	163	41.1	225	455.6	267	34.5	340	473.5	1004.7

hydrogen desorption represented by the peak areas were only 2.2 and 4.1% of the total hydrogen desorption, respectively. The amount of hydrogen desorption of type γ adsorption on Cu was only 3.7% of the total hydrogen desorption. Therefore, a new type of adsorption site (γ) was found after ZrO_2 doping. However, the amounts of desorbed hydrogen on type α and type γ adsorption sites were very minimal and thus have a limited influence on the catalytic hydrogenation activity. In type β and type δ sites, the adsorption amounts of H_2 remarkably increased after ZrO_2 doping, particularly in the type β site, which was 3.6 times on the peak area of the Cu–Fe sample. ZrO_2 doping had a significant effect on the H_2 adsorption amount at sites β and δ. These results indicate that H_2 adsorption on the Cu surface is dissociative when CO_2 hydrogenation to DME occurs between 240 and 280°C.[16] H_2 is especially adsorbed on the type β site. Evidently, the temperature of hydrogen desorption from the Cu–Fe–Zr catalyst was higher than that from the corresponding Cu–Fe sample, which indicates a higher ability of the Cu–Fe–Zr catalyst to activate H_2. As a result, stronger metal–hydrogen bonds are formed.[40] Cu and Fe components were better dispersed in the Cu–Fe–Zr sample than in the Cu–Fe sample, which was attributed to the presence of ZrO_2.[41] Thus, more unsaturated coordination metal centers were present, which formed strong bonds with H_2.[38,40,42] Furthermore, the degree of H_2 adsorption corresponded to catalytically useful adsorption strength. Adding 1.0 wt % ZrO_2 to the catalyst improves the bimetallic interaction of Cu and Fe, thereby enhancing the catalytic performance in the hydrogenation reaction. For the Cu–Fe–Zr catalysts, the adsorption of H_2 on ZrO_2 cannot be detected. Nonetheless, the strength of H_2 adsorption to Cu and Fe surface moieties can be adjusted by Zr-doping.

CO_2-TPD. After *in situ* reduction at 300°C, CO_2-TPD on CuO, Fe_2O_3, Cu–Fe, and Cu–Fe–Zr (containing 1.0 wt % ZrO_2) catalysts were carried out to investigate the nature of CO_2 adsorption onto their surfaces. The results are shown in Figure 3.

In Figure 3, there are two obvious CO_2 desorption peaks from the CuO sample, and three coincident CO_2 desorption peaks on the Fe_2O_3, Cu–Fe, and Cu–Fe–Zr catalysts. In this case, a higher temperature CO_2 desorption peak indicates a higher basicity of the adsorption center. As such, the three CO_2 desorption peaks correspond successively to weakly basic sites (98–300°C), medium-strength basic sites (400–500°C), and strongly basic sites (600°C), respectively. Again, the low content of ZrO_2 present in the Cu–Fe–Zr catalysts effectively rendered the adsorption of CO_2 to this component unobservable. To weakly basic sites, CO_2 adsorbed in a linear fashion (O=C=O—M), whereas on the medium strength and strongly basic sites, CO_2 adsorbed in a bridge type configuration $\left(\mathrm{C}{<}^{\mathrm{O-M}}_{\mathrm{O-M}}\right)$.[43] This bridging configuration was formed by the adsorption of each oxygen in CO_2 to the metal catalyst surface, which makes the stripping of the adsorbed CO_2 more difficult and raises the desorption temperature to 400–500°C in the case of moderately basic adsorption sites and to 600°C for removal from strongly basic sites.

In this study, the catalytic hydrogenation of CO_2 to DME was carried out between 240 and 280°C, and for this reason, most of the CO_2 was linearly adsorbed onto weakly basic sites. The CO_2 desorption peak of the CuO sample is not obvious, indicating that CO_2 adsorbs very weakly to the weakly basic sites on the Cu surface. Obvious CO_2 desorption peaks were found on the Fe_3O_4, Cu–Fe, and Cu–Fe–Zr samples between 50 and 280°C, which suggests that CO_2 adsorbs primarily to the Fe_3O_4 species in the Cu–Fe-based catalysts.[16,36] Desorption of CO_2 from the weak base sites on the Cu–Fe and Cu–Fe–Zr samples were located at 103 and 98°C, respectively. Thus, Zr-doping can be used to modulate the temperature at which CO_2 adsorbs to the weakly basic sites on Cu–Fe catalysts, and may facilitate desorption of CO_2, from the catalyst surface. Additionally, the area of CO_2 desorption peak increased on Zr-doping, which indicated that ZrO_2 doping increases the CO_2 adsorption capacity of the doped catalysts compared to a Cu–Fe catalyst. The Cu–Fe–Zr catalyst catalytically activates more CO_2 than the undoped catalyst, favoring an improvement in its ability to catalyze the hydrogenation of CO_2 to DME.[24]

Adsorption state of CO_2 molecules on Cu(111) plane

In this study, Cu-metal oxide was used as the catalyst for the methanol synthesis reaction. Due to the complexity of the active sites and reaction intermediates, there are

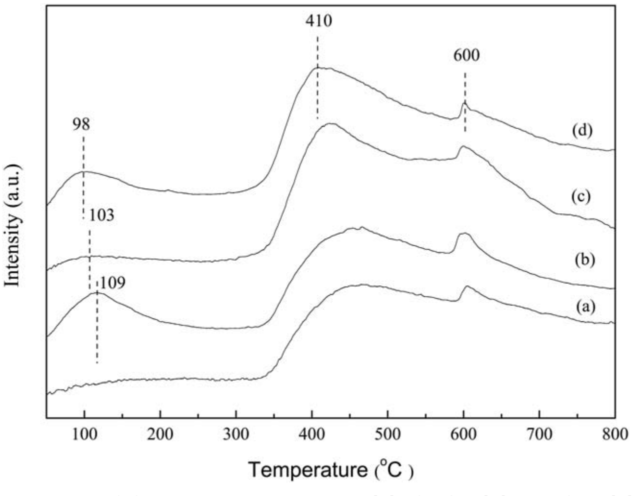

Figure 3. CO_2-TPD profiles for (a) CuO, (b) Fe_2O_3, (c) Cu–Fe, (d) Cu–Fe–Zr (ZrO_2 = 1.0 wt %) after hydrogenation.

Table 2. Optimized Energetic Results for the System of CO_2 Adsorbed on Cu(111)

Absorption Site on Cu(111) Plane	Molecular Orientation of CO_2	$E_{(CO_2)}$ (kJ·mol^{-1})	$E_{(surface)}$ (kJ·mol^{-1})	$E_{(CO_2/surface)}$ (kJ·mol^{-1})	E_{ads} (kJ·mol^{-1})
Top	Horizontal	−495,221.59	−9,335,978.94	−9,831,208.22	−7.69
	Vertical			−9,831,205.34	−4.81
Bridge	Horizontal			−9,831,209.23	−8.70
	Vertical			−9,831,205.26	−4.73
fcc	Horizontal			−9,831,205.23	−4.69
	Vertical			−9,831,208.84	−8.31
hcp	Horizontal			−9,831,205.24	−4.70
	Vertical			−9,831,208.75	−8.21

controversies regarding the identity of the adsorption site and the adsorbed state of CO_2 on the Cu surface during the process of methanol synthesis.[44,45] Therefore, studying the reaction mechanism of methanol synthesis on Cu-based catalysts at the atomic level, establishing the geometric configurations of the Cu-containing active sites and of the reaction intermediates, simulating, and calculating the elementary steps comprising the reaction mechanism, and elucidating the reaction kinetics and thermodynamics of the reaction process are important objectives to address to design an effective catalyst for the overall synthesis of DME from CO_2.

CO_2-TPD analysis revealed that CO_2 adsorbed onto the weak base centers of Cu surfaces with an atop configuration and in the linear O═C═O form, resulting in desorption peaks in the range of 240–280°C for the Cu–Fe–Zr catalyst. By considering the four types of adsorption sites on a Cu(111) plane and the two possible molecular orientations for CO_2 adsorption, eight models describing the adsorption of linear CO_2 onto a Cu(111) plane were constructed to theoretically determine the most energetically stable structure. To minimize the energy of each model, all eight models of adsorption were geometrically optimized by a DMol^3 module calculated with full electronic. The adsorption energies of the eight structural models for CO_2 adsorbed on a Cu(111) plane are shown in Table 2.

As shown in Table 2, the adsorption energies of CO_2 onto the Cu(111) plane for all configurations are negative, indicating that the total energy of the system decreased on CO_2 adsorption to the surface, and furthermore that CO_2 can be readily adsorbed onto Cu(111). CO_2 horizontally adsorbed to a bridging Cu(111) site yields the lowest adsorption energy of all configurations (−8.70 kJ·mol^{-1}), and therefore, reveals this to be the optimal adsorption configuration. However, when CO_2 is horizontally adsorbed on the bridging site, the bond angle is 179.75°, and the length of C═O bond is 0.1172 nm, both of which are nearly equivalent to their values before adsorption (180° and 0.1174 nm, respectively), which further indicates that CO_2 spontaneously adsorbs on Cu(111) plane in this fashion but also that the adsorption interaction is weak. According to generally accepted interpretations of adsorption energy, adsorption energies with a magnitude of approximately 8–20 kJ·mol^{-1} constitute a physical adsorption event.[46] According to the CO_2-TPD results, Fe_3O_4 shows higher adsorption capacity than Cu at 240–280°C, as well as stronger adsorption of CO_2 to its surface.[46–48] Additionally, H_2-TPD results showed that between 240 and 280°C, dissociative adsorption of H_2 primarily occurred on Cu. In many DFT calculations,[47–49] it has been found that Cu-based catalyst that have been doped with transition metal oxide additives adsorb H_2 by dissociative adsorption onto Cu, while the transition metal oxides adsorb and activate CO_2. Subsequent CO_2 desorb from the metal oxide surface and adsorb to metallic Cu to allow the adsorbed species to react with dissociated H at the Cu site; this causes the deformation activation of O═C═O linear configurations.

Process of methanol synthesis from CO_2 on Cu(111) plane

Utilizing Cu-based catalysts, methanol may be synthesized from CO_2 and H_2 by two pathways, one being the formic acid pathway. In this way, CO_2 reacts with dissociatively adsorbed H on the Cu surface to form a bidentate HCOO intermediate, and the HCOO is hydrogenated a second time to generate various intermediates of formic acid (HCOOH); these HCOOH intermediates are subsequently hydrogenated to generate CH_2O, CH_3O, and CH_3OH. As the name suggests, adsorbed isomers of formic acid are the main intermediates in this pathway. The other mechanistic pathway is the CO pathway: due to the occurrence of the reverse water–gas shift reaction and methanol synthesis in parallel, CO intermediates generated by the former can be hydrogenated to produce methanol. CO is the main intermediate in this pathway. Furthermore, based on this pathway, one may infer that CO is the main by-product of methanol synthesis. Methanol, then, may be synthesized from CO_2 over Cu(111) by two types of pathways, through both a formate intermediate and through reverse water–gas shift-mediated CO hydrogenation. The details of these pathways are shown in Eqs. 5 and 6, in which * denotes an adsorption site and TS signifies the transition state.

$$\begin{aligned} &CO_2+6H^* \rightarrow HCOO^{**}+5H^* \rightarrow TS1 \rightarrow HCOOH^{**}+4H^* \rightarrow TS2\\ &\rightarrow H_2CO^{**}+2H^*+H_2O \rightarrow TS7 \rightarrow H_3CO^*+H^*+H_2O\\ &\rightarrow TS8 \rightarrow CH_3OH^*+H_2O \rightarrow CH_3OH+H_2O \end{aligned} \tag{5}$$

$$\begin{aligned} &CO_2+6H^* \rightarrow TS3 \rightarrow HOCO^{**}+5H^* \rightarrow TS4 \rightarrow CO^*\\ &+4H^*+H_2O \rightarrow TS5 \rightarrow HCO^*+3H^*+H_2O \rightarrow TS6\\ &\rightarrow H_2CO^{**}+2H^*+H_2O \rightarrow TS7 \rightarrow H_3CO^*+H^*\\ &+H_2O \rightarrow TS8 \rightarrow CH_3OH^*+H_2O \rightarrow CH_3OH+H_2O \end{aligned} \tag{6}$$

Deferring to these two pathways, DFT was used to simulate the process of methanol synthesis from CO_2 and H_2 on Cu(111). The resultant optimized molecular structures of reactant, transition state, and product are shown in Figures 4–6.

As shown in Figure 4, in the catalytic reaction system, molecular H_2 is first catalytically activated by dissociation into two H atoms on the Cu(111) plane, which separately

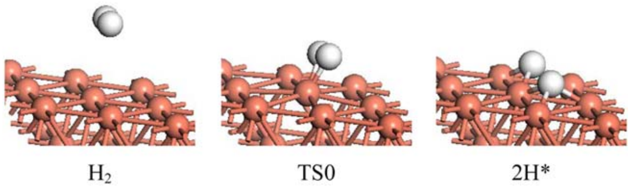

Figure 4. The process simulation of the dissociative adsorption of H_2 on Cu(111) (brown, Cu; gray, C; red, O; white, H).

[Color figure can be viewed in the online issue, which is available at wileyonlinelibrary.com.]

occupy one adsorption site in what is denoted the TS0 transition state. The dissociative adsorption energy of H_2 was obtained by Eq. 7

$$E_{\text{ads}} = E_{(H_2/\text{surface})} - E_{(H_2)} - E_{(\text{surface})} \tag{7}$$

Here, $E_{(H_2/\text{surface})}$ denotes the total dissociation energy of H_2 on the Cu(111) plane, $E_{(H_2)}$ denotes the energy of the H_2 molecule, and $E_{(\text{Surface})}$ is the energy of the Cu(111) plane.

The DMol^3 calculation results indicate that the first step in methanol synthesis involves the dissociative adsorption of molecular H_2 on the Cu(111) plane, which is an exothermic process having an adsorption energy (E_{ads}) of -94.51 kJ·mol^{-1}. Because this energy is higher than 8–20 kJ·mol^{-1}, it is an indication that H_2 can be stably chemisorbed onto Cu(111), which is in agreement with the H_2-TPD results presented in the third section.

The CO_2 adsorbed to the surface, which desorbed from Fe_3O_4, directly reacted with the chemisorbed atomic H in a horizontally bound linear configuration. The mechanism for methanol synthesis via the formic acid pathway is shown in Figure 5. HCOO is directly generated from CO_2 and H without a transition state, the geometry of the CO_2 being distorted to generate HCOO in this way. HCOO occupies two adsorption sites in a bridging interaction with the Cu(111) plane and is from this point hydrogenated to form methanol.

Methanol synthesis by way of CO formation as catalyzed by Cu(111) is outlined in Figure 6. HOCO is generated from CO_2 and H through the TS3 transition state, and as the hydroxyl-containing HOCO intermediate is a constitutional isomer of HCOO, the linear type CO_2 is essentially activated to HCOO and is then hydrogenated to methanol.

The elementary reaction processes, reaction energy barriers for the reaction processes, and the potential energies corresponding to Figures 4–6 are shown in Table 3. A diagram of the potential energy surface of the reaction process is shown in Figure 7 as well as the energies derived from analysis that correspond to methanol formation through HCOO and HOCO intermediates.

Because the elementary reactions comprising the two methanol synthesis pathways are different, the energy changes of the two processes are also very different. The dissociative adsorption of H_2 on the Cu(111) plane is spontaneous and exothermic, and as such exists presents a TS0 transition state during the conversion process that in turn forms a reaction energy barrier of 91.96 kJ·mol^{-1}. A surface chemical reaction takes place directly between dissociated H and CO_2 species, and both a formate isomer (HCOO: both O bound to Cu, occupying two Cu surface sites) and a carboxyl isomer (HOCO: one O and C to the Cu surface, occupying two active sites). The formic acid pathway itself includes no transition state, and the HCOO formed as a result of it is the stable intermediate species. The energy barrier of HCOO is $E_a = 107.86$ kJ·mol^{-1}, and so the change in energy by its formation is $\Delta E = -24.94$ kJ·mol^{-1}, making it an exothermic transformation. The HCOO is then hydrogenated to the formate species, which is an endothermic process, where $E_a = 166.31$ kJ·mol^{-1} and $\Delta E = 72.22$ kJ·mol^{-1}. The surface-adsorbed formic acid is then hydrogenated to methanol.

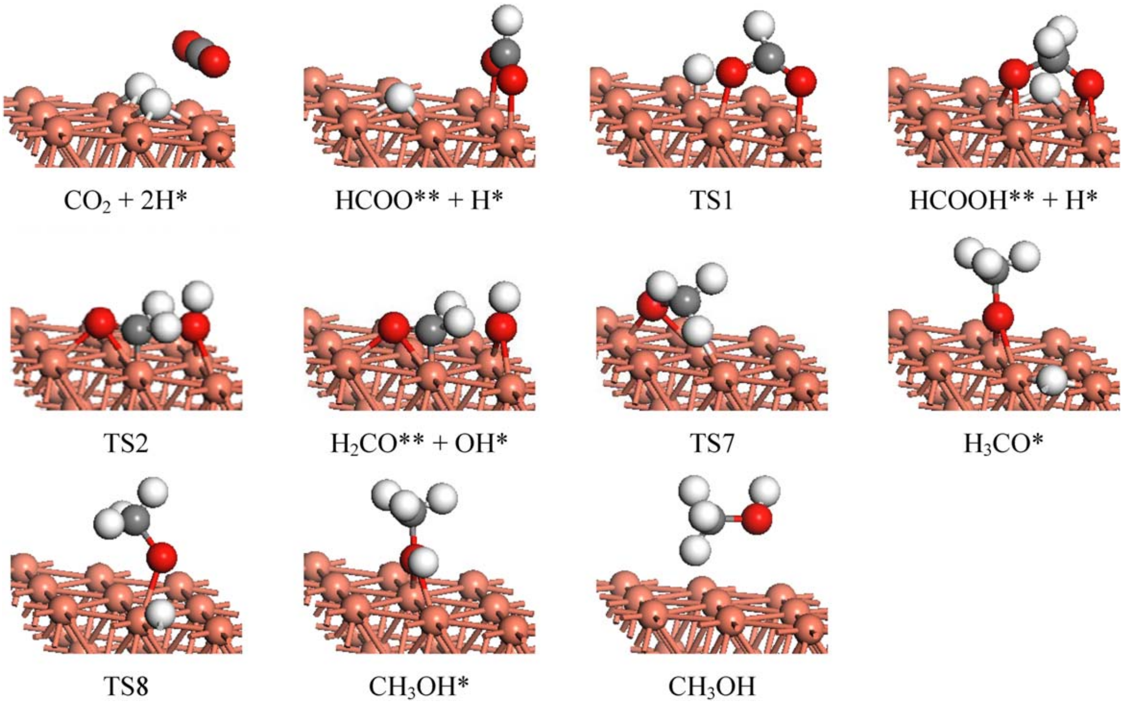

Figure 5. The process simulation of the methanol synthesis reaction from CO_2 hydrogenation on Cu(111) via the formate pathway(brown, Cu; gray, C; red, O; white, H).

[Color figure can be viewed in the online issue, which is available at wileyonlinelibrary.com.]

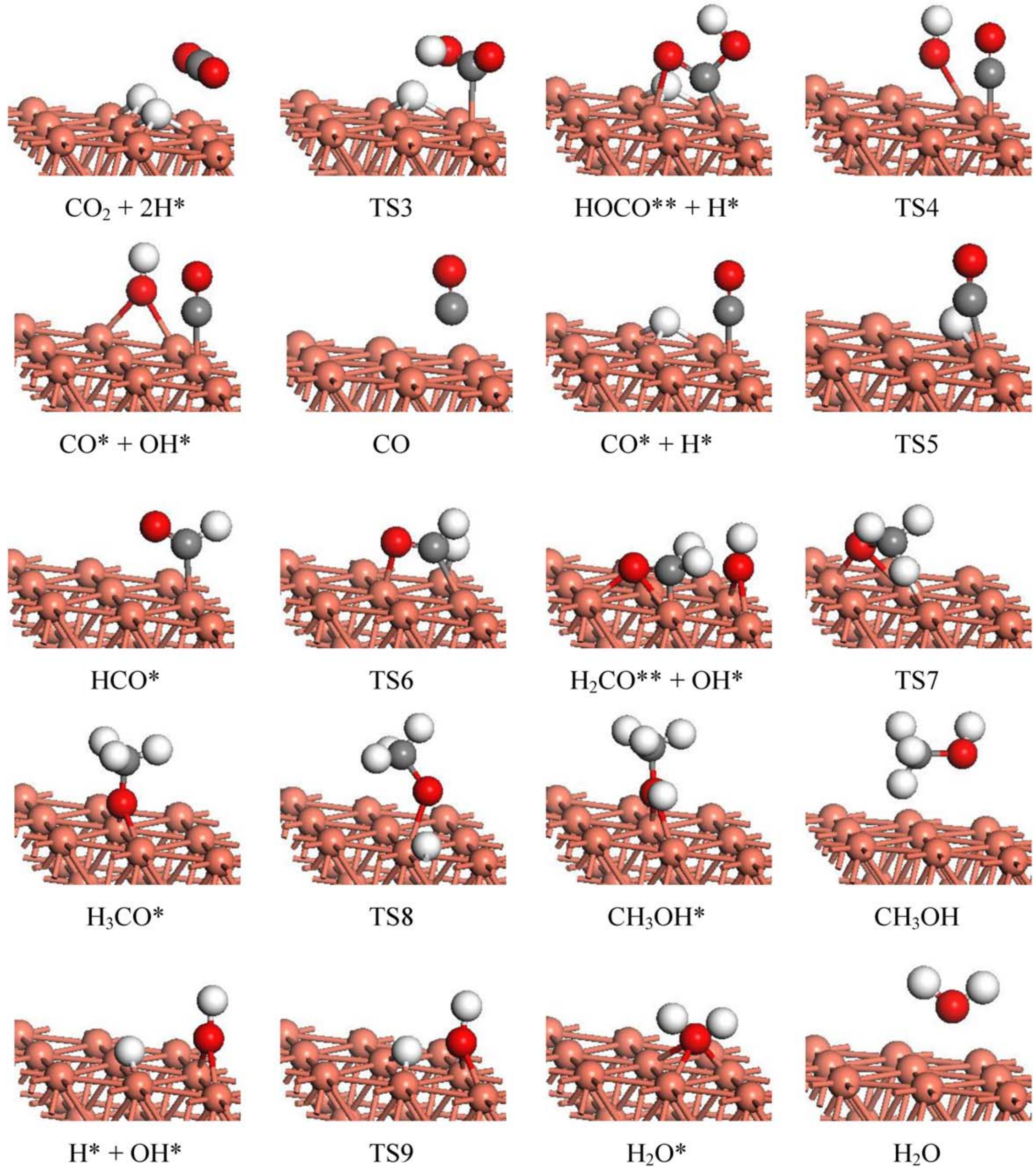

$CO_2 + 2H^*$ TS3 $HOCO^{**} + H^*$ TS4

$CO^* + OH^*$ CO $CO^* + H^*$ TS5

HCO^* TS6 $H_2CO^{**} + OH^*$ TS7

H_3CO^* TS8 CH_3OH^* CH_3OH

$H^* + OH^*$ TS9 H_2O^* H_2O

Figure 6. The process simulation of the methanol synthesis reaction from CO_2 hydrogenation on Cu(111) via the CO hydrogenation pathway (brown, Cu; gray, C; red, O; white, H).

[Color figure can be viewed in the online issue, which is available at wileyonlinelibrary.com.]

For the CO pathway, the imaginary frequency of CO_2 hydrogenation to form HOCO is $-1503.13\ cm^{-1}$, indicating the existence of a transition state in this conversion step. The adsorption energy of HOCO is $E_a = 161.67\ kJ{\cdot}mol^{-1}$ and $\Delta E = -8.41\ kJ{\cdot}mol^{-1}$. Once formed, HOCO is hydrogenated and the carboxyl breaks to form OH* and CO*. There is a second transition state formed as the hydrogenated HOCO breaks to form CO. This is an overall exothermic reaction step, with $E_a = 50.46\ kJ{\cdot}mol^{-1}$ and $\Delta E = -1.59\ kJ{\cdot}mol^{-1}$, and from this point the resultant CO is hydrogenated to methanol.

Comparing the formic acid pathway and CO pathway, the energy barrier to CO generation is lower than that for formic acid production ($50.46\ kJ{\cdot}mol^{-1} < 166.31\ kJ{\cdot}mol^{-1}$). Furthermore, the generation of CO is an exothermic process, whereas process of formic acid generation is an endothermic one, underlining that CO is easier to produce than formic acid. The produced CO will be successively hydrogenated to HCO, H_2CO, and H_3CO to finally obtain methanol.

The molecular simulations of the forward and reverse reactions of CO hydrogenation to HCO are compared in Figure 8, and the changes of potential energy that occur in the process are shown in Figure 9.

In the forward reaction (Figure 8), the imaginary frequency of HCO production by CO hydrogenation is $-970.79\ cm^{-1}$, revealing the existence of a transition state. The reaction energy barrier formed is $E_a = 106.32\ kJ{\cdot}mol^{-1}$ and $\Delta E = 58.70\ kJ{\cdot}mol^{-1}$, and so it is an endothermic process. In the reverse reaction, however, there is no transition state formed as HCO decomposes into CO and H, and the reaction energy barrier is $E_a = 13.43\ kJ{\cdot}mol^{-1}$, which is

Table 3. The Elementary Steps of the Methanol Synthesis Reaction

Elementary Steps	E_a (kJ·mol^{-1})	ΔE (kJ·mol^{-1})	Frequency (cm^{-1})
$H_2 + 2^* \rightleftharpoons 2H^*$	91.96	−19.92	−775.53
$H^* + CO_2 \rightleftharpoons HCOO^{**}$	107.86	−24.94	–
$HCOO^{**} + H^* \rightleftharpoons HCOOH^{**} + {}^*$	166.31	72.22	−934.54
$HCOOH^{**} + H^* \rightleftharpoons H_2CO^{**} + OH^*$	177.99	−37.36	−60.38
$H^* + CO_2 \rightleftharpoons HOCO^{**}$	161.67	−8.41	−1503.13
$HOCO^{**} \rightleftharpoons CO^* + OH^*$	50.46	−1.59	−248.51
$CO^* \rightleftharpoons CO + {}^*$	86.61	86.61	–
$CO^* + H^* \rightleftharpoons HCO^* + {}^*$	106.32	58.70	−970.79
$HCO^* + {}^* \rightleftharpoons CO^* + H^*$	13.43	−58.70	–
$HCO^* + H^* \rightleftharpoons H_2CO^{**}$	72.59	−19.96	−918.80
$H_2CO^{**} + H^* \rightleftharpoons H_3CO^* + 2^*$	48.45	−97.19	−20.67
$H_3CO^* + H^* \rightleftharpoons CH_3OH^* + {}^*$	96.57	−23.35	−987.09
$CH_3OH^* \rightleftharpoons CH_3OH + {}^*$	29.00	29.00	–
$H^* + OH^* \rightleftharpoons H_2O^* + {}^*$	127.57	−5.98	−1008.53
$H_2O^* \rightleftharpoons H_2O$	16.36	16.36	–

approximately eight times smaller than that of the forward process, rendering it exothermic ($\Delta E = -58.70$ kJ·mol^{-1}). Overall, the formation of CO by CO_2 hydrogenated is more easily accomplished than formate generation. However, HCO cannot exist in the reaction system steadily, as the HCO generated by CO hydrogenation is prone to decomposition back into CO, causing the accumulation of CO in the system, and inhibiting the conversion of CO into methanol. Therefore, it is reasonable to infer that CO_2 hydrogenation to methanol occurs primarily through the formic acid pathway.

A sequential list of the intermediates formed in the complete hydrogenation of CO_2 by the formate pathway includes HCOO, HCOOH, H_2CO, CH_3O, and CH_3OH with energy barriers (E_a) of 107.86, 166.31, 177.99, 48.45, and 96.57 kJ·mol^{-1}, respectively. The ΔE on formation of these intermediates are 24.94, 17.26, −37.36, −97.19, and −23.35 kJ·mol^{-1}, respectively. The energy barrier resulting from the hydrogenation of HCOOH to form H_2CO is the largest, and it is an exothermic reaction, indicating that this elementary reaction, shown in Eq. 8, is the rate-limiting step.

$$HCOOH^{**} + H * \rightleftharpoons H_2CO^{**} + OH^* \tag{8}$$

Reverse water–gas shift reactions can result in both HOCO and CO formation from CO_2. The reaction energy barriers to the formation of these intermediates are 161.67 and 50.46 kJ·mol^{-1}, respectively, and from this one may conclude that CO_2 hydrogenation to form HOCO is the rate-limiting step in the conversion of CO_2 by the reverse water–gas shift reaction on Cu(111), as elucidated in Eq. 9

$$H^* + CO_2 \rightleftharpoons HOCO^{**} \tag{9}$$

Study of intrinsic kinetics

Exclude the Internal and External Diffusion. The Cu–Fe–Zr/HZSM-5 catalyst was used in the catalytic hydrogenation of CO_2 to DME, and the effects of the mass of catalyst used (1.0 and 2.0 g) and the residence time on catalytic performance were investigated. The results are shown in Figure 10. When the residence time is less than 1.0×10^{-3} h^{-1}, namely, the space velocity is more than 1500 mL·g_{cat}^{-1}·h^{-1}, the CO_2 conversion curves when 1.0 g and 2.0 g catalyst are loaded, tested at several residence times, all overlap, which indicated that CO_2 conversion is not be affected by the gas mass flow rate. Therefore, when the space velocity is more than 1500 mL·$g_{cat}{}^{-1}$·h^{-1}, the influence of mass-transfer resistance of external diffusion to the reaction can be ignored.

Once external diffusion was excluded as a relevant factor, the influence of Cu–Fe–Zr/HZSM-5 particle size on CO_2 conversion was investigated, and the result is shown in Figure 11. When the average catalyst particle size is 0.15–0.42 mm (or 20–100 mesh), the average CO_2 conversion rate is 28%, which shows that in this size range CO_2 conversion is not affected by the catalyst particle size, and thus, mass-transfer resistance of the internal diffusion can be ignored. Therefore, in the catalytic reaction system, when the space velocity is more than 1500 mL·$g_{cat}{}^{-1}$·h^{-1} and the particle size is less than 20 mesh, the reaction of CO_2 hydrogenated to DME is not affected by mass-transfer resistance to internal or external diffusion, and instead is controlled by intrinsic kinetic processes.

Suggested Mechanism of CO_2 Hydrogenation to DME. In the catalytic CO_2 hydrogenation to DME, a Cu–Fe–Zr/HZSM-5 dual-function catalyst was used for CO_2 hydrogenation, with the target products being DME and methanol; the expected by-products are CO and CH_4. Due to the reaction energy barrier of CH_4 formation being less than those of DME and methanol formation, as well as that of the

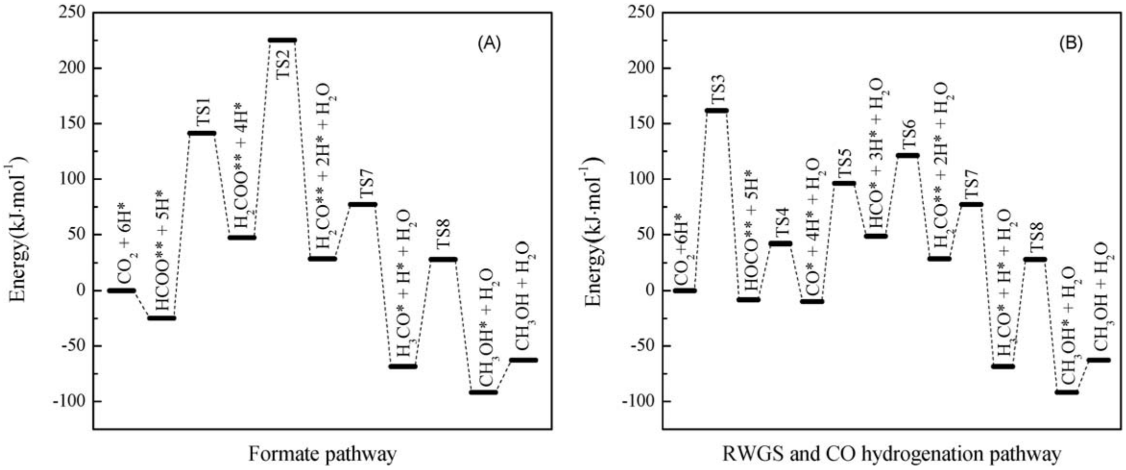

Figure 7. Potential energy diagrams for the methanol synthesis reaction via the formate(A) and CO(B) hydrogenation pathways.

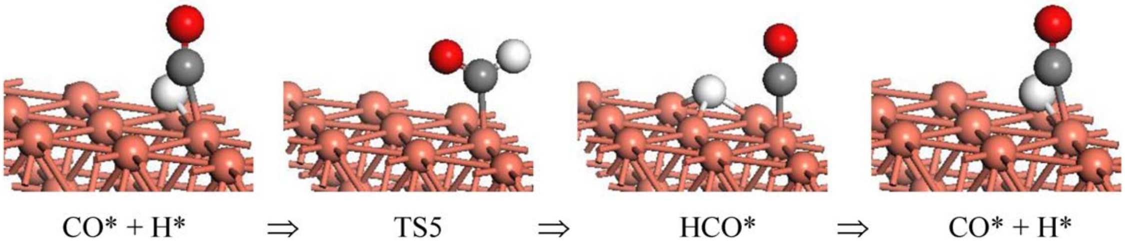

Figure 8. The elementary step of CO* + H* ⇌ HCO* + * (brown, Cu; gray, C; red, O; white, H).

[Color figure can be viewed in the online issue, which is available at wileyonlinelibrary.com.]

reverse water–gas reaction,[6] and considering that the observed CH_4 yield is less than 1%, CH_4 synthesis is considered to be balanced with the reaction of CO_2 hydrogenation to DME.

To investigate the intrinsic kinetics of Cu–Fe–Zr/HZSM-5 catalyzed CO_2 hydrogenation to DME, three reactions should be considered: methanol synthesis, methanol dehydration to DME, and the reverse water–gas shift reaction, which are shown in Eqs. 1–3.

The methanol synthesis and reverse water–gas reactions were carried out over the Cu–Fe–Zr catalyst, and methanol dehydration to DME occurred on the HZSM-5 component of the catalyst.

Methanol synthesis and methanol dehydration are consecutive, exothermic reactions, signifying that methanol is an important reaction intermediate in the synthesis of DME from CO_2. Furthermore, methanol synthesis and the reverse water–gas shift reaction are mutually parallel reactions, and so the CO formed by the latter process affects the former. The active sites and the rate-limiting step of the methanol synthesis reaction are still controversial. Numerous studies[6,25–29] show that Cu is the main active site in methanol synthesis over Cu-based catalysts and that when doped by other metal oxides, the dispersion, stability, and electronic properties of copper active sites can be altered, improving the activity of Cu and leading to improved catalytic performance of the copper-based catalyst. According to the results of H_2-TPD and CO_2-TPD presented earlier, H_2 adsorbs easily to Cu whereas CO_2 adsorption onto Cu is weak at 240–280°C and is primarily achieved by adsorption to Fe and subsequent desorbed and moved to Cu. In methanol synthesis, the small amount of doped ZrO_2 (1.0 wt %) serves to strengthen the adsorption interactions of the Cu–Fe catalyst and to increase the number of active sites on the catalyst surface. It is supposed that adsorbed CO_2 molecules directly react with the H that was previously adsorbed on the Cu surface. In this way, CO_2 is hydrogenated to form formic acid (HCOO), which is then hydrogenated to form a series of intermediates species in sequence, including H_2COO, CH_2O, and CH_3O, respectively, the last of which is finally converted to methanol. The generation of the intermediate species is considered to be rate-limiting step.

In synthesizing DME by way of methanol dehydration, the adsorbed methanol obtains a proton (H) adsorbed at the acid sites of HZSM-5. Following a unimolecular nucleophilic substitution reaction scheme,[50] the methanol molecule dissociates into a positive carbon ion and water, and a neighboring, undissociated methanol combines with the carbon cation as a nucleophile, forming DME. The suggested reaction mechanisms of CO_2 hydrogenation to DME are shown in Eqs. 10–26, where * indicates single atomic adsorption, ** represents diatomic adsorption, and HX signifies HZSM-5.

The CO_2 hydrogenation and reverse water–gas reactions are shown in Eqs. 10–21

$$H_2+2^{*}\rightleftharpoons 2H^{*} \tag{10}$$

$$CO_2+H^{*}+{}^{*}\rightleftharpoons HOCO^{**} \tag{11}$$

$$HOCO^{**}\rightleftharpoons CO^{*}+OH^{*} \tag{12}$$

$$CO^{*}\rightleftharpoons CO+{}^{*} \tag{13}$$

$$CO_2+H^{*}+{}^{*}\rightleftharpoons HCOO^{**} \tag{14}$$

$$HCOO^{**}+H^{*}\rightleftharpoons HCOOH^{**}+{}^{*} \tag{15}$$

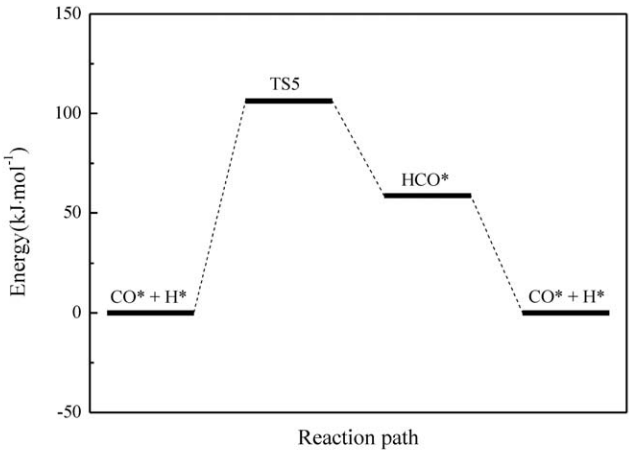

Figure 9. The potential energy diagram of the elementary step of CO* + H* ⇌ HCO* + *.

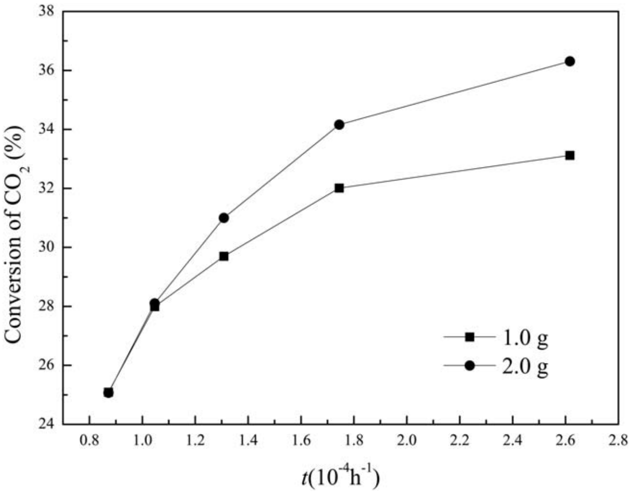

Figure 10. The changes of CO_2 conversion with the residence time.

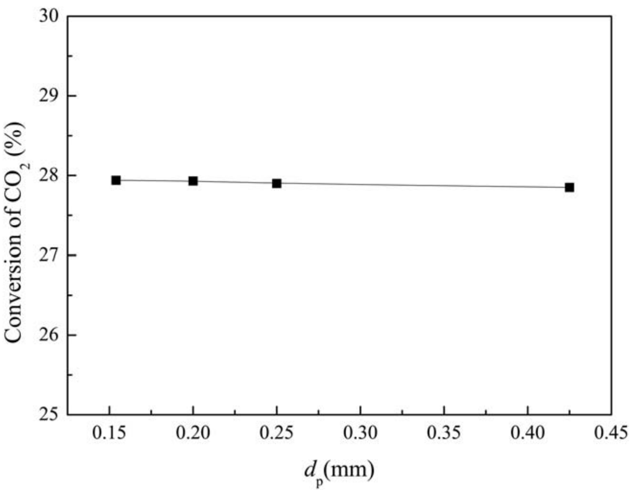

Figure 11. The changes of CO_2 conversion with the catalyst particle sizes.

$$HCOOH^{**}+H* \rightleftharpoons H_2CO^{**}+OH^{*} \qquad (16)$$

$$H_2CO^{**}+H^{*} \rightleftharpoons H_3CO^{*}+2^{*} \qquad (17)$$

$$H_3CO^{*}+H^{*} \rightleftharpoons CH_3OH^{*}+^{*} \qquad (18)$$

$$CH_3OH^{*} \rightleftharpoons CH_3OH+^{*} \qquad (19)$$

$$H^{*}+OH^{*} \rightleftharpoons H_2O^{*}+^{*} \qquad (20)$$

$$H^{*}+OH^{*} \rightleftharpoons H_2O^{*}+^{*} \qquad (21)$$

The reactions of methanol dehydration to DME are shown in Eqs. 22–26.

$$CH_3OH+HX \rightleftharpoons HX\ CH_3OH \qquad (22)$$

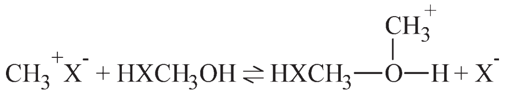
(23)

$$CH_3{}^{+}X^{-} + HXCH_3OH \rightleftharpoons HXCH_3—\overset{\overset{CH_3^{+}}{|}}{O}—H + X^{-} \qquad (23)$$

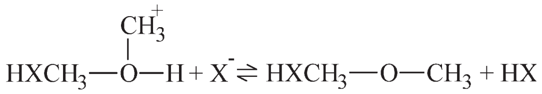
(24)

$$HXCH_3—\overset{\overset{CH_3^{+}}{|}}{O}—H + X^{-} \rightleftharpoons HXCH_3—O—CH_3 + HX \qquad (24)$$

$$HXCH_3—O—CH_3 \rightleftharpoons CH_3OCH_3+HX \qquad (25)$$

$$H^{+}+X^{-} \rightleftharpoons HX \qquad (26)$$

To the reaction mechanism for CO_2 hydrogenation to methanol, Zhao et al.[51] suggested that direct formate hydrogenation does not lead to methanol due to the high hydrogenation barriers of HCOO and H_2COO; and Behrens et al.[52] suggested the hydrogenation of CO_2 proceeded via formation of HCOO, HCOOH, and H_2COOH, and methanol formation via the methoxy (CH_3O) intermediate. And in the suggested mechanism in this study, the hydrogenation of CO_2 proceeded via formation of HOCO, HCOO, HCOOH, and methanol formation via CH_3O, which is similar to the suggestion from Behrens and can be used in the following study.

Derivation of the Intrinsic Kinetics Model. The catalytic hydrogenation of CO_2 to DME over Cu–Fe–Zr/HZSM-5 was carried out in a differential fixed-bed reactor, which can be regarded as a plug flow system, and a gas–solid catalyzed reaction system. According to the dynamic Langmuir–Hinshelwood chemisorption model,[53,54] we assume that:

1. When the Cu–Fe–Zr/HZSM-5 was used as a catalyst, Cu species acted as the active site for the water–gas reaction and methanol synthesis;
2. HZSM-5 is the active site for methanol dehydration;
3. Chemical adsorption, surface reaction, and desorption are occurred exclusively on these two active sites;
4. The concentrations of the gaseous and liquid forms of each component present in the reaction system reach equilibrium, and the gases behave as ideal gases;
5. The rate-limiting step of the reverse water–gas reaction is Eq. 11, and controlling the rate of methanol synthesis is Eq. 16, and the rate-limiting step of methanol dehydration is Eq. 23, and in each case, the nonrate-controlling steps reach equilibrium.

According to these assumptions, four intrinsic kinetic models of CO_2 hydrogenation to DME were established, and kinetic equations for these are shown in Table 4.

The Estimation of Intrinsic Kinetic Parameters and Model Discrimination. According to atomic matrix method, the number of the independent reactions involved in CO_2 conversion to DME was three, which indicates in turn that three key chemical components exist in the reaction. We assumed CO_2, CO, and DME to be the three components, and chemical reaction rate equations were established as shown in Eqs. 27–30.

Table 4. Intrinsic Kinetics Models of Different Rate Determining Steps (RDS)

Reaction	Model	RDS	Model Equation[a]
Reverse water-gas shift reaction		(11)	$r_A=\frac{k_A p_{CO_2} p_{H_2}^{0.5}[1-(K_A/K_{PA})(p_{CO}p_{H_2O}/p_{CO_2}p_{H_2})]}{(1+K_{CO}p_{CO}+K_{H_2O}p_{H_2O})^2}$
Hydrogenation of CO_2	Model 1	(14)	$r_B=\frac{k_B p_{CO} p_{H_2O}[1-(K_B/K_{PB})(p_{CH_3OH}/p_{CO}p_{H_2}^{2})]}{(1+K_{CO}p_{CO}+K_{H_2O}p_{H_2O})^3}$
	Model 2	(15)	$r_B=\frac{k_B p_{CO} p_{H_2O}[1-(K_B/K_{PB})(p_{CH_3OH}/p_{CO}p_{H_2}^{1.5})]}{(1+K_{CO}p_{CO}+K_{H_2O}p_{H_2O})^3}$
	Model 3	(16)	$r_B=\frac{k_B p_{CO}[1-(K_B/K_{PB})(p_{CH_3OH}/p_{CO}p_{H_2}^{0.5})]}{(1+K_{CO}p_{CO}+K_{H_2O}p_{H_2O})^3}$
	Model 4	(17)	$r_B=\frac{k_B p_{CO} p_{H_2}^{2.5}[1-(K_B/K_{PB})(p_{CH_3OH}/p_{CO}p_{H_2}^{2.5})]}{(1+K_{CO}p_{CO}+K_{H_2O}p_{H_2O})^3}$
Methanol dehydration to DME		(23)	$r_C=\frac{k_C[p_{CH_3OH}^2/p_{H_2O}-(K_3/K_{PC})p_{DME}]}{(1+K_{CH_3OH}p_{CH_3OH}+K'_{H_2O}p_{H_2O})^2}$

[a]The subscript of A, B, C represent for reverse water-gas shift reaction, hydrogenation of CO_2 reaction, and methanol dehydration to DME reaction, respectively.

Table 5. Intrinsic Kinetic Data of the Catalytic Hydrogenation of CO_2 to DME

T (°C)	P(MPa)	W_{cat}/ϕ_V (10^{-3}g$_{cat.}$·h·m^{-3})	p_{CO_2} (MPa)	p_{CO} (MPa)	p_{DME} (MPa)	p_{CH_3OH} (MPa)	p_{H_2O} (MPa)	p_{H_2} (MPa)
240	3.0	2.0	0.4346	0.0042	0.0298	0.0197	0.1285	2.3832
240	3.0	2.4	0.4336	0.0046	0.0312	0.0180	0.1307	2.3819
240	3.0	3.0	0.4321	0.0053	0.0329	0.0161	0.1336	2.3800
240	3.0	4.0	0.4297	0.0067	0.0352	0.0138	0.1380	2.3766
250	3.0	2.0	0.4321	0.0107	0.0189	0.0482	0.1222	2.3679
250	3.0	2.4	0.4290	0.0103	0.0273	0.0373	0.1323	2.3637
250	3.0	3.0	0.4253	0.0107	0.0349	0.0286	0.1424	2.3580
250	3.0	4.0	0.4199	0.0127	0.0425	0.0219	0.1548	2.3481
260	3.0	2.0	0.4262	0.0099	0.0358	0.0244	0.1416	2.3622
260	3.0	2.4	0.4217	0.0119	0.0406	0.0225	0.1510	2.3523
260	3.0	3.0	0.4163	0.0145	0.0459	0.0212	0.1621	2.3400
260	3.0	4.0	0.4074	0.0196	0.0526	0.0222	0.1787	2.3196
270	3.0	2.0	0.4423	0.0045	0.0107	0.0421	0.1057	2.3948
270	3.0	2.4	0.4353	0.0049	0.0265	0.0228	0.1259	2.3846
270	3.0	3.0	0.4264	0.0089	0.0362	0.0174	0.1444	2.3667
270	3.0	4.0	0.4082	0.0185	0.0506	0.0230	0.1799	2.3198
280	3.0	2.0	0.4499	0.0041	0.0023	0.0364	0.0854	2.4218
280	3.0	2.4	0.4424	0.0087	0.0226	0.0191	0.1060	2.4013
280	3.0	3.0	0.4249	0.0153	0.0329	0.0195	0.1394	2.3678
280	3.0	4.0	0.3975	0.0216	0.0454	0.0283	0.1944	2.3129
260	2.0	4.0	0.2728	0.0131	0.0321	0.0109	0.1157	1.5553
260	2.5	4.0	0.3337	0.0204	0.0453	0.0184	0.1588	1.9234
260	3.0	4.0	0.4084	0.0189	0.0520	0.0218	0.1768	2.3221
260	3.5	4.0	0.4973	0.0100	0.0445	0.0156	0.1688	2.7638

$$r_{CO_2}=-\frac{\mathrm{d}[(y_{CO_2,\mathrm{in}}-y_{CO_2,\mathrm{out}})P/RT]}{\mathrm{d}(W_{\mathrm{cat}}/\phi_{\mathrm{V}})} \tag{27}$$

$$r_{CO}=\frac{\mathrm{d}(y_{CO,\mathrm{out}}P/RT)}{\mathrm{d}(W_{\mathrm{cat}}/\phi_{\mathrm{V}})} \tag{28}$$

$$r_{DME}=\frac{\mathrm{d}(y_{DME,\mathrm{out}}P/RT)}{\mathrm{d}(W_{\mathrm{cat}}/\phi_{\mathrm{V}})} \tag{29}$$

$$y_i=p_i/P \tag{30}$$

The relationships between the reaction rate equations and kinetic equations were established based on the mass balance as shown in Eqs. 31–33.

$$r_{CO_2}=-r_A-r_B \tag{31}$$

$$r_{CO}=r_{\mathrm{A}} \tag{32}$$

$$r_{DME}=2r_{\mathrm{C}} \tag{33}$$

The nonlinear least-square optimization method was used to estimate the intrinsic kinetic parameters and discriminate the models, using the square residual of the experimental values and the calculated values of partial pressure for each component as the optimized objective function; this is shown in Eq. 34.

$$\Phi=\sum_{i=1}^{n}[(p_{CO_2,\mathrm{exp}}-p_{CO_2,\mathrm{cal}})^2+(p_{CO,\mathrm{exp}}-p_{CO,\mathrm{cal}})^2+(p_{DME,\mathrm{exp}}-p_{DME,\mathrm{cal}})^2] \tag{34}$$

Fourth- and fifth-order Runge–Kutta algorithms were used to obtain the optimal solution to ordinary differential Eqs. 27–29. The optimization algorithm was established using Matlab programming (MathWorks, R2010b version), and Levenberg–Marquart damped least-squares optimization[55] was carried out by lsqnonlin subroutines. Ode45 subroutines were used to solve the system of ordinary differential equations. And substituting in the experimental data, several iterations were carried out to obtain the minimum of the target function value, that is, the estimated parameter value of the intrinsic kinetics and the residual sum of squares within the 95% confidence interval were obtained. Because the preexponential factor, activation energy, adsorption equilibrium constant, and adsorption heat are only a function of temperature, there are strong correlations between the preexponential factor and the activation energy, and between the adsorption equilibrium constant and the adsorption heat. When the equilibrium constants k_i or K_i corresponding to each reaction temperature were substituted for, the Arrhenius equation and the Van't Hoff equations transformed into Eqs. 35 and 36, respectively.

$$k_i(T)=k_{i,0}\exp\left(-\frac{E_i}{RT}\right)\rightarrow k_i(T)=k_{i,0}\exp\left[-\frac{E_i}{R}\left(\frac{1}{T}-\frac{1}{T_0}\right)\right] \tag{35}$$

$$k_i(T)=k_{i,0}\exp\left(-\frac{\Delta H_i}{RT}\right)\rightarrow k_i(T)=k_{i,0}\exp\left[-\frac{\Delta H_i}{R}\left(\frac{1}{T}-\frac{1}{T_0}\right)\right] \tag{36}$$

The experimental intrinsic kinetic data for catalytic CO_2 hydrogenation to DME are shown in Table 5.

The optimized model parameters of the intrinsic kinetics are shown in Table 6.

Based on the residual sum of squares Φ, decisive indicator ρ^2, and the F-test value, the calculation formulas are shown in Eqs. 34, 37, and 38, and the optimal intrinsic kinetic model was screened.

$$\text{Decisive index:}\quad \rho^2=1-\sum_{i=1}^{M}(y_{i,\mathrm{exp}}-y_{i,\mathrm{cal}})^2\bigg/\sum_{i=1}^{M}y_{i,\mathrm{exp}}^2 \tag{37}$$

$$F\text{-value:}\quad F=\frac{\left[\sum_{i=1}^{M}y_{i,\mathrm{exp}}^2-\sum_{j=1}^{M}(y_{i,\mathrm{exp}}-y_{i,\mathrm{cal}})^2\right]/M_p}{\sum_{i=1}^{M}(y_{i,\mathrm{exp}}-y_{i,\mathrm{cal}})^2/(M-M_{\mathrm{p}})} \tag{38}$$

where, $y_{j,\mathrm{exp}}$ and $y_{j,\mathrm{cal}}$ are the experimental values and calculated model values of CO yield and DME yield, respectively;

Table 6. Intrinsic Kinetic Parameters of the Catalytic Hydrogenation of CO_2 to DME

Kinetic Constant	Model 1	Model 2	Model 3	Model 4
$k_{A,0}$[a] ($mol \cdot h^{-1} \cdot MPa^{-1.5} \cdot g^{-1}$)	9.12	6.65	6.58	6.65
$k_{B,0}$	4.31×10^3 ($mol \cdot h^{-1} \cdot MPa^{-2} \cdot g^{-1}$)	5.94×10^2 ($mol \cdot h^{-1} \cdot MPa^{-2} \cdot g^{-1}$)	2.83×10^3 ($mol \cdot h^{-1} \cdot MPa^{-1} \cdot g^{-1}$)	69.21 ($mol \cdot h^{-1} \cdot MPa^{-3.5} \cdot g^{-1}$)
$k_{C,0}$ ($mol \cdot h^{-1} \cdot MPa^{-1} \cdot g^{-1}$)	1.69×10^3	1.05×10^3	1.53×10^3	1.05×10^3
E_A ($kJ \cdot mol^{-1}$)	119.33	108.66	109.16	105.65
E_B ($kJ \cdot mol^{-1}$)	124.10	149.41	173.72	224.35
E_C ($kJ \cdot mol^{-1}$)	90.21	85.86	89.91	109.08
$K_{CO,0}$[b] (MPa^{-1})	1.16×10^4	3.46×10^{-9}	1.16×10^4	9.68×10^{-8}
$K_{H_2O,0}$ (MPa^{-1})	3.02×10^{-5}	3.96×10^{-8}	3.00×10^{-5}	1.11×10^{-6}
$K'_{H_2O,0}$ (MPa^{-1})	3.24×10^2	4.44×10^{-11}	3.25×10^2	4.44×10^{-11}
K_{CH_3OH} (MPa^{-1})	5.62×10^2	4.44×10^{-11}	5.50×10^2	4.44×10^{-11}
$-\Delta H_{CO}$ ($kJ \cdot mol^{-1}$)	83.55	62.17	66.19	162.84
$-\Delta H_{H_2O}$ ($kJ \cdot mol^{-1}$)	23.30	136.77	25.82	12.18
$-\Delta H'_{H_2O}$ ($kJ \cdot mol^{-1}$)	56.78	33.64	44.52	46.02
$-\Delta H_{CH_3OH}$ ($kJ \cdot mol^{-1}$)	101.59	5.98	54.43	40.84
Φ	1.35×10^{-3}	3.34×10^{-3}	1.00×10^{-3}	2.54×10^{-3}
ρ^2	0.9997	0.9992	0.9998	0.9994
F-Statistic	1749.70	527.79	1762.83	693.67

[a,b]The subscript 0 indicates the value at 260°C.

M_p is the number of variables; and M is the experiment time.

Comparing the four intrinsic kinetics models, the residual sum of squares of model 3 is 1.00×10^{-3}, and the decisive index is the largest ($0.9998 > 0.99$), indicating that the total deviation of regression value of model 3 is the smallest, and the calculated value of the model was much better matched to the experimental data than the other models. Therefore, model 3 was selected as the optimal intrinsic kinetics model for Cu–Fe–Zr/HZSM-5 catalyzed hydrogenation of CO_2 to DME. In model 3, the activation energies of the reverse water–gas shift reaction, methanol synthesis, and methanol dehydration to DME were found to be 109.16, 173.72, and 89.91 $kJ \cdot mol^{-1}$, respectively. This suggests that synthesis of methanol is the bottleneck in the production of DME from CO_2. The rate-limiting steps of the reverse water–gas shift, methanol synthesis, and methanol dehydration reactions are given in Eqs. 11, 16, and 23.

The rate-limiting steps of methanol synthesis and the reverse water–gas reaction as confirmed by molecular simulation-based calculations were in agreement with the results of the intrinsic kinetics experiment. Therefore, the assumptions made in the elucidation of the intrinsic kinetics are supported. The reaction activation energies of methanol synthesis and the reverse water–gas reaction extracted from the molecular simulation are 177.99 and 161.67 $kJ \cdot mol^{-1}$, and the values calculated from the intrinsic kinetic model are only slightly different, at 173.72 and 109.16 $kJ \cdot mol^{-1}$. The reason for this is that the methanol synthesis and reverse water–gas reactions are not independent of one another in this particular catalytic reaction system.

Validation of the Intrinsic Kinetics Model. The F-test was used to validate intrinsic kinetics model 3, for which $10F_{0.05}(M_p, M-M_p) = 2.74$, and which yielded $F = 1762.83 > 10F_{0.05}$, indicating that the experimental results predicted by model 3 were more reasonable at $\alpha = 0.05$. The experimental values of the partial pressures of CO_2, CO, and DME were plotted against the values calculated by model 3, and the residual analysis of the experimental and calculated values is shown in Figure 12. In the analysis diagram, the points are evenly distributed on both sides of the diagonal, which support the reliability of model 3. The experimental data of CO_2 conversion at different reaction temperatures and space velocities was plotted against the results calculated from model 3 and is shown in Figure 13. The experimental data branched away from and rejoined the fitting curve, and the relative errors between the calculated and experimental data of the partial pressures of all components were less than

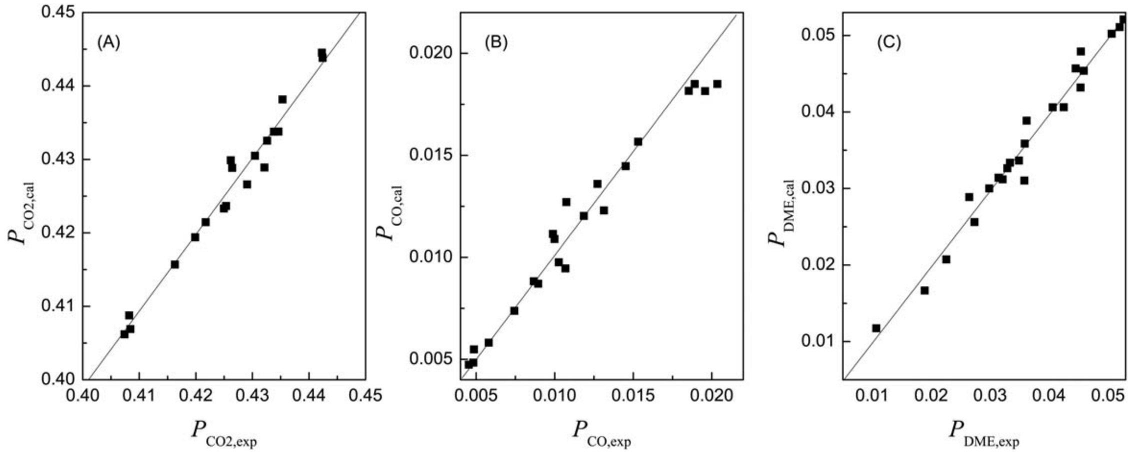

Figure 12. Fitting between the experimental values of the gas partial pressures of CO_2(A), CO(B), DME(C) and the values calculated with kinetic model 3.

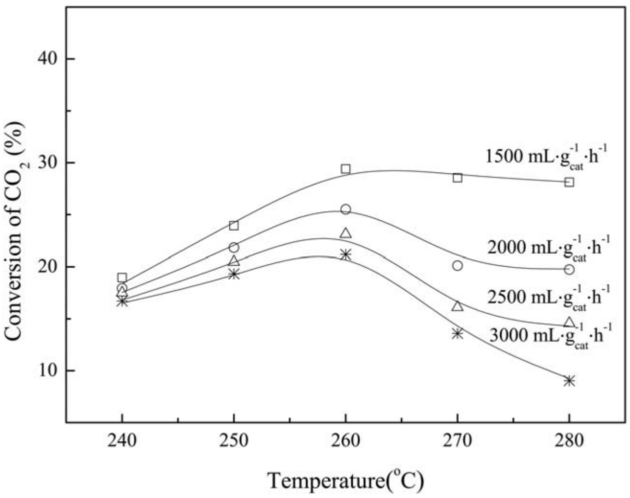

Figure 13. Results for the conversions of CO_2 at different temperatures and space velocities, under 3.0 MPa, $V(H_2)/V(CO_2) = 5$.

Points represent experimental results. Lines represent calculated results with kinetic model 3.

10%, such that the kinetics model may be considered an accurate descriptor of the intrinsic kinetics of CO_2 hydrogenation to DME.

Conclusions

The adsorption state of CO_2 on a Cu(111) plane and the methanol synthesis reaction were studied using DFT, and the intrinsic kinetics of DME synthesis from CO_2 was investigated, resulting in the establishment of an intrinsic kinetic model. The main conclusions of this work are the following:

1. The adsorption state of CO_2 on Cu(111) plane was studied by subjecting eight adsorption configurations of CO_2 on a Cu(111) plane to DFT analysis, and the optimal adsorption configuration was found to be that of linear CO_2 adsorbed in a bridging conformation with its axis of symmetry parallel to the Cu(111) plane. The adsorption energy of CO_2 in this case was -8.70 kJ·mol^{-1}, and signified CO_2 is physisorbed rather than chemisorbed to the active site. H_2 was dissociatively adsorbed onto Cu(111) plane through a stable chemisorption interaction, exhibiting a dissociative adsorption energy of -94.50 kJ·mol^{-1}. Fe_3O_4 was regarded as a catalytic promoter, and CO_2 adsorbed to Cu from Fe_3O_4. Additionally, the activation of linear-type CO_2 occurred directly by the reaction of an adsorbed CO_2 molecule and dissociatively adsorbed H on the Cu surface.

2. Molecular simulation was used to study the two possible pathways of methanol synthesis from CO_2 and H_2. The simulation result indicated that methanol synthesis from CO_2 proceeded via the formate pathway, and CO also accumulated in the process. The rate-determining steps of the reverse water–gas shift reaction and the methanol synthesis reaction occurred when catalyzed by Cu(111) plane were Eqs. 9 and 8, respectively. The reaction energy barriers of the above two reactions were 161.67 and 177.99 kJ·mol^{-1}, respectively.

3. The intrinsic kinetics of the mechanism for DME synthesis from CO_2 was investigated and the intrinsic kinetic model was established, which was based on the reverse water–gas shift reaction, the methanol synthesis reaction, and the dehydration of methanol to DME. The activation energy of the methanol synthesis reaction was the largest of the three at 173.72 kJ·mol^{-1}, and so it was concluded that methanol synthesis was the apparent rate-limiting step in the catalyzed transformation of CO_2 to DME. The rate-determining elementary step of the above three basic reactions was in Eq. 16. And the relative errors between the calculated and experimental data of the partial pressures of all components were less than 10%, the kinetics model may be considered an accurate descriptor of the intrinsic kinetics of CO_2 hydrogenation to DME.

Acknowledgment

This work was supported by National Natural Science Foundation of China (21006013, 21425627), Guangxi Zhuang Autonomous Region special funding of distinguished experts, and the Open Project of Guangxi Key Laboratory of Petrochemical Resource Processing and Process Intensification Technology (2013K012).

Notation

X_i = conversion, mol%
S_i = selectivity, mol%
Y_i = yield, mol%
y_i = mole fraction of component *i*, mol%
P = total pressure, MPa
p_i = partial pressure of component *i*, MPa
W_{cat} = weight of the catalyst, g
r = reaction rate, mol·h^{-1}·g^{-1}
k = reaction rate constant
K = adsorption constant, MPa^{-1}
E_a = activation energy, kJ·mol^{-1}
E = potential energy, kJ·mol^{-1}
ΔE = energy change, kJ·mol^{-1}
ΔH = adsorption enthalpy increment, kJ·mol^{-1}
T = temperature, K
ΔG^{θ} = standard Gibbs free energy, kJ·mol^{-1}
R = gas constant, J·mol^{-1}·K^{-1}
ϕ_V = volumetric flow rate, mol·h^{-1}
V = volumetric flow rate, mL·min^{-1}
Φ = residual square sum
ρ^2 = determinant index
F = *F*-test value
α = confidence

Subscripts

i = the *i*th component
0 = the value at 260°C
out = flow out
cal = calculation value
exp = experimental value
RWGS = reverse water–gas shift reaction
M = methanol synthesis
DME = methanol dehydration to DME
cat = catalyst
V = gas

Superscripts

θ = standard condition

Literature Cited

1. Arcoumanis C, Bae C, Crookes R, Kinoshita E. The potential of dimethyl ether (DME) as an alternative fuel for compression-ignition engines: a review. *Fuel*. 2008;87(7):1014–1030.
2. Semelsberger TA, Borup RL, Greene HL. Dimethyl ether (DME) as an alternative fuel. *J Power Sources*. 2006;156(2):497–511.
3. Olah GA, Goeppert A, Prakash GKS. Chemical recycling of carbon dioxide to methanol and dimethyl ether: from greenhouse gas to

renewable, environmentally carbon neutral fuels and synthetic hydrocarbons. *J Org Chem.* 2008;74(2):487–498.

4. Wang W, Wang S, Ma X, Gong J. Recent advances in catalytic hydrogenation of carbon dioxide. *Chem Soc Rev.* 2011;40(7):3703–3727.
5. Centi G, Perathoner S. Opportunities and prospects in the chemical recycling of carbon dioxide to fuels. *Catal Today.* 2009;148(3–4):191–205.
6. Ereña J, Sierra I, Aguayo AT, Ateka A, Olazar M, Bilbao J. Kinetic modelling of dimethyl ether synthesis from ($H_2 + CO_2$) by considering catalyst deactivation. *Chem Eng J.* 2011;174(2–3):660–667.
7. Jia G, Tan Y, Han Y. A comparative study on the thermodynamics of dimethyl ether synthesis from CO hydrogenation and CO_2 hydrogenation. *Ind Eng Chem Res.* 2006;45(3):1152–1159.
8. Sosna MK, Sokolinskii YA, Shovkoplyas NY, Korolev EV. Application of the thermodynamic method to developing the process of producing methanol and dimethyl ether from synthesis gas. *Theor Found Chem Eng.* 2007;41(6):809–815.
9. Naik SP, Du H, Wan H, Bui V, Miller JD, Zmierczak WW. A comparative study of $ZnO-CuO-Al_2O_3/SiO_2-Al_2O_3$ composite and hybrid catalysts for direct synthesis of dimethyl ether from syngas. *Ind Eng Chem Res.* 2008;47(23):9791–9794.
10. Rahimpour MR, Farniaei M, Abbasi M, Javanmardi J, Kabiri S. Comparative study on simultaneous production of methanol, hydrogen, and DME using a novel integrated thermally double-coupled reactor. *Energy Fuels.* 2013;27(4):1982–1993.
11. Zhao Y, Chen J, Zhang J. Effects of ZrO_2 on the performance of CuO-ZnO-Al_2O_3/HZSM-5 catalyst for dimethyl ether synthesis from CO_2 hydrogenation. *J Nat Gas Chem.* 2007;16(4):389–392.
12. Naik SP, Ryu T, Bui V, Miller JD, Drinnan NB, Zmierczak W. Synthesis of DME from CO_2/H_2 gas mixture. *Chem Eng J.* 2011;167(1):362–368.
13. Tao J-L, Jun K-W, Lee K-W. Co-production of dimethyl ether and methanol from CO_2 hydrogenation: development of a stable hybrid catalyst. *Appl Organomet Chem.* 2001;15(2):105–108.
14. Qi G-X, Fei J-H, Zheng X-M, Hou Z-Y. DME synthesis from carbon dioxide and hydrogen over Cu–Mo/HZSM-5. *Catal Lett.* 2001;72(1–2):121–124.
15. Yang H-x, Jia L-s, Fang W-p, Li Q-b. Study on catalytic activity of Cu-Mn/HZSM-5 catalyst for dimethyl ether synthesis. *Nat Gas Chem Ind.* 2008;33(1):1–5.
16. Wang S, Mao D-S, Guo X-M, Lu G-Z. Dimethyl ether synthesis from CO_2 hydrogenation over CuO-TiO_2-ZrO_2/HZSM-5 catalyst. *Acta Phys Chim Sin.* 2011;27(11):2651–2658.
17. Arena F, Italiano G, Barbera K, Bonura G, Spadaro L, Frusteri F. Basic evidences for methanol-synthesis catalyst design. *Catal Today.* 2009;143(1–2):80–85.
18. Toyir J, de la Piscina PR, Llorca J, Fierro J-LG, Homs N. Methanol synthesis from CO_2 and H_2 over gallium promoted copper-based supported catalysts. Effect of hydrocarbon impurities in the CO_2/H_2 source. *Phys Chem Chem Phys.* 2001;3(21):4837–4842.
19. Lee S, Sardesai A. Liquid phase methanol and dimethyl ether synthesis from syngas. *Top Catal.* 2005;32(3–4):197–207.
20. Xie D, Fan F. Process conditions for methanolization and methanation purification of ammonia synthesis feed gas. *Chem Ind Eng Prog.* 2006;25(7):833–836.
21. Ko JB, Bae CM, Jung YS, Kim DH. Cu–ZrO_2 catalysts for water-gas-shift reaction at low temperatures. *Catal Lett.* 2005;105(3–4):157–161.
22. Zhang Q, Zuo Y-Z, Han M-H, Wang J-F, Jin Y, Wei F. Long carbon nanotubes intercrossed Cu/Zn/Al/Zr catalyst for CO/CO_2 hydrogenation to methanol/dimethyl ether. *Catal Today.* 2010;150(1–2):55–60.
23. Lim H-W, Park M-J, Kang S-H, Chae H-J, Bae JW, Jun K-W. Modeling of the Kinetics for methanol synthesis using Cu/ZnO/Al_2O_3/ZrO_2 catalyst: influence of carbon dioxide during hydrogenation. *Ind Eng Chem Res.* 2009;48(23):10448–10455.
24. Liu R-W, Qin Z-Z, Ji H-B, Su T-M. Synthesis of dimethyl ether from CO_2 and H_2 using a Cu–Fe–Zr/HZSM-5 catalyst system. *Ind Eng Chem Res.* 2013;52(47):16648–16655.
25. Iliuta I, Larachi F, Fongarland P. Dimethyl ether synthesis with in situ H_2O removal in fixed-bed membrane reactor: model and simulations. *Ind Eng Chem Res.* 2010;49(15):6870–6877.
26. Sierra I, Ereña J, Aguayo AT, Olazar M, Bilbao J. Deactivation kinetics for direct dimethyl ether synthesis on a $CuO-ZnO-Al_2O_3/\gamma$-Al_2O_3 catalyst. *Ind Eng Chem Res.* 2009;49(2):481–489.
27. McBride K, Turek T, Güttel R. Direct dimethyl ether synthesis by spatial patterned catalyst arrangement: a modeling and simulation study. *AlChE J.* 2012;58(11):3468–3473.
28. Wang J-Y, Wang X-H, Zeng C-Y, Wu C-Z. Intrinsic kinetics of dimethyl ether synthesis directly from CO_2 hydrogenatin. *Acta Petrolei Sin.* 2007;23(1):62–68.
29. Wang X-H, Wang J-Y, Zeng C-Y. Kinetics of dimethyl ether synthesis from CO_2 hydrogenation. *Nat Gas Chem Ind.* 2005;30(1):17–20.
30. Nørskov JK, Bligaard T, Rossmeisl J, Christensen CH. Towards the computational design of solid catalysts. *Nat Chem.* 2009;1(1):37–46.
31. Cramer CJ, Truhlar DG. Density functional theory for transition metals and transition metal chemistry. *Phys Chem Chem Phys.* 2009;11(46):10757–10816.
32. Crljen Ž, Lazić P, Šokčević D, Brako R. Relaxation and reconstruction on (111) surfaces of Au, Pt, and Cu. *Phys Rev B.* 2003;68(19):195411.
33. Furmaniak S, Kowalczyk P, Terzyk AP, Gauden PA, Harris PJF. Synergetic effect of carbon nanopore size and surface oxidation on CO_2 capture from CO_2/CH_4 mixtures. *J Colloid Interface Sci.* 2013;397:144–153.
34. Bhatia SK, Nguyen TX. Potential of silicon carbide-derived carbon for carbon capture. *Ind Eng Chem Res.* 2011;50(17):10380–10383.
35. Agrell J, Birgersson H, Boutonnet M, Melián-Cabrera I, Navarro RM, Fierro JLG. Production of hydrogen from methanol over Cu/ZnO catalysts promoted by ZrO_2 and Al_2O_3. *J Catal.* 2003;219(2):389–403.
36. Niemelä M, Nokkosmäki M. Activation of carbon dioxide on Fe-catalysts. *Catal Today.* 2005;100(3–4):269–274.
37. Lin H, Duan X, Zheng J, Zheng X, He P, Yuan Y, Yang Y. Vapor-phase hydrogenation of dimethyl oxalate over a CNTs-Cu-SiO_2 hybrid catalyst with enhanced activity and stability. *RSC Adv.* 2013;3(29):11782–11789.
38. Yang X, Wei Y, Su Y, Zhou L. Characterization of fused Fe–Cu based catalyst for higher alcohols synthesis and DRIFTS investigation of TPSR. *Fuel Process Technol.* 2010;91(9):1168–1173.
39. Zhou M, Lin G, Zhang H. Pt catalyst supported on multiwalled carbon nanotubes for hydrogenation-dearomatization of toluene. *Chin J Catal.* 2007;28(3):210–216.
40. Zhang J-X, Zhao Y-Q, Chen J-X, Wang R-J, Zhang J-Y. Study on direct synthesis of dimethyl ether by hydrogenation of carbon dioxide: I. effects of precipitaion agent on structure and properties of catalyst. *J Fuel Chem Technol.* 2003;31(5):444–448.
41. Bin F, Song C, Lv G, Song J, Wu S, Li X. Selective catalytic reduction of nitric oxide with ammonia over zirconium-doped copper/ZSM-5 catalysts. *Appl Catal B.* 2014;150:532–543.
42. Wang F-Y, Huang J-S, Xu Y-D, Dai L-Z, Lu D-X, Peng S-Y. A comparative study on Cu-Co catalysts differing in preparation for the synthesis of lower alcohols II. H_2-TPD, CO-TPD and CO/H_2 TPSR. *Chin J Catal.* 1994;15(6):426–431.
43. Wang J-Y, Zeng C-Y, Lin L. Effect of promoters on the catalytic performance and properties of Cu-ZnO-Al_2O_3-SiO_2 catalysts. *J Petrochem Univ.* 2006;18(3):9–14.
44. Tao X-M, Sun J-L, Liu W-J, Ye Q-G, Li Z-W. Quantum chemical simulation on the reaction of methanol synthesis from CO_2 and H_2. *Nat Gas Chem Ind.* 2013;38(3):57–61.
45. Xiao W, Ten L, Lu W. Progress in the study of the mechanism and kinetics of synthesis of methanol and DME from syngas. *Petrochem Technol.* 2004;33(6):497–507.
46. Yang Y, Evans J, Rodriguez JA, White MG, Liu P. Fundamental studies of methanol synthesis from CO_2 hydrogenation on Cu(111), Cu clusters, and Cu/ZnO($000\bar{1}$). *Phys Chem Chem Phys.* 2010;12(33):9909–9917.
47. Schumacher N, Boisen A, Dahl S, Gokhale AA, Kandoi S, Grabow LC, Dumesic JA, Mavrikakis M, Chorkendorff I. Trends in low-temperature water–gas shift reactivity on transition metals. *J Catal.* 2005;229(2):265–275.
48. Tang Q-L, Hong Q-J, Liu Z-P. CO_2 fixation into methanol at Cu/ZrO_2 interface from first principles kinetic Monte Carlo. *J Catal.* 2009;263(1):114–122.
49. Yang Y, White MG, Liu P. Theoretical study of methanol synthesis from CO_2 hydrogenation on metal-doped Cu(111) surfaces. *J Phys Chem C.* 2011;116(1):248–256.
50. Ouellette RJ, Rawn JD. 10 - nucleophilic substitution and elimination reactions. In: Ouellette RJ, Rawn JD, editors. Organic Chemistry. Boston: Elsevier, 2014:333–356.

51. Zhao YF, Yang Y, Mims C, Peden CHF, Li J, Mei DH. Insight into methanol synthesis from CO_2 hydrogenation on Cu(111): complex reaction network and the effects of H_2O. *J Catal.* 2011;281(2):199–211.
52. Behrens M, Studt F, Kasatkin I, Kühl S, Hävecker M, Abild-Pedersen F, Zander S, Girgsdies F, Kurr P, Kniep B-L, Tovar M, Fischer RW, Nørskov JK, Schlögl R. The active site of methanol synthesis over Cu/ZnO/Al_2O_3 industrial catalysts. *Science*. 2012; 336(6083):893–897.
53. Armenise S, Garcia-Bordeje E, Valverde JL, Romeo E, Monzon A. A Langmuir-Hinshelwood approach to the kinetic modelling of catalytic ammonia decomposition in an integral reactor. *Phys Chem Chem Phys*. 2013;15(29):12104–12117.
54. Kumar KV, Porkodi K, Rocha F. Langmuir–Hinshelwood kinetics—A theoretical study. *Catal Commun.* 2008;9(1):82–84.
55. Fazlollahi F, Sarkari M, Gharebaghi H, Atashi H, Zarei MM, Mirzaei AA, Hecker WC. Preparation of Fe-Mn/K/Al_2O_3 Fischer-Tropsch catalyst and its catalytic kinetics for the hydrogenation of carbon monoxide. *Chin J Chem Eng*. 2013;21(5):507–519.

Manuscript received July 27, 2014, and revision received Jan. 9, 2015.